Study of MIMO Control Laws for Seismic Isolation of Flexible Payload

Jennifer Watchi[1], Binlei Ding[1], Guoying Zhao[1] and Christophe Collette[1,2]

Abstract— In order to operate properly, some precision applications need to be isolated from the ground motion in the six degrees of freedom. This paper presents the model of a hexagonal payload which is isolated in all directions. The model is validated by comparison with experimental data. It reproduces properly the suspension modes and the flexibilities of the structure. Two multi-input multi-output (MIMO) control techniques have been applied to this system: centralized control and singular value decomposition (SVD). Both methods allow to reduce by a factor 100 the transmission of ground motion at low frequency (up to 5 Hz) without interfering with the flexible modes.

I. INTRODUCTION

The transmission of ground motion to sensitive equipment can affect their performance or their resolution. To overcome this limitation, passive and active isolation solutions have been developed. When it is supported by springs, a system is isolated passively in a frequency range above its resonance frequency. Those springs can be pneumatic elements [1], [2] or mechanical springs [3]. On the other hand, feedback control, one type of active isolation, consists of sensing the motion of the system to isolate and canceling this motion by injecting a force that opposes this motion [4]. To increase the performance, passive solutions can be combined with feedback control [5].

For some applications, like atomic gravimeters [11] or gravitational waves detectors [7], the system has to be isolated in more than one direction. By isolating several directions in parallel, the force used to control one direction can inject some spurious signal to another direction. Therefore, to cope with this coupling between different directions, instead of considering each direction independently, a global approach is used. Two multi-input multi-output (MIMO) control methods commonly used are the centralized control [3], [8] and the singular value decomposition (SVD) method [9].

These solutions can be tested on a model to predict their performance. Most of the models developed include only the rigid body modes of a system [10]. However, in practice, the flexibilities of a structure represent a main limitation when isolating a system. In fact, if the gain of the controller is too large, the crossover frequency can be larger than the flexible modes and some of them can be amplified.

In this paper, a finite element model (FEM) of a hexagonal table, representing the system to isolate, is introduced. For calculation cost's reasons [11], a reduced model of this system containing the first 60 modes is extracted from the FEM. The two MIMO approaches are then defined and the feedback controllers are designed on the model. The performance of SVD and centralized controllers are compared on the reduced model. Finally, the model is validated by comparison with experimental data.

II. DESCRIPTION OF THE FINITE ELEMENT MODEL

The FEM represents a hexagonal table which is 15 cm high and 75 cm along each side, see Fig. 1. The payload weights 157 kg. It is supported by three pairs of vertical and horizontal springs with a stiffness of 3 kN/m. To add more passive isolation to the system, the whole structure lays on a rectangular table of 1 m x 2 m which weights 330 kg. It is connected to the ground by four vertical springs with a stiffness of 90 kN/m.

Frequency analysis is carried out to identify the resonance frequencies and the corresponding mode shapes of the system. The first 60 modes of the system are then retained to generate a reduced model of the FEM [12], [13]. These 60 modes include the six suspension modes of the hexagonal table, between 0.6 Hz and 1.5 Hz, the six suspension modes of the rectangular table, between 5 Hz and 8 Hz, and the first 48 flexible modes of both tables, between 70 Hz and 600 Hz. This decoupling between rigid and flexible modes will ease the controller design as the crossover frequency can be set between these two types of resonances, around 10 Hz.
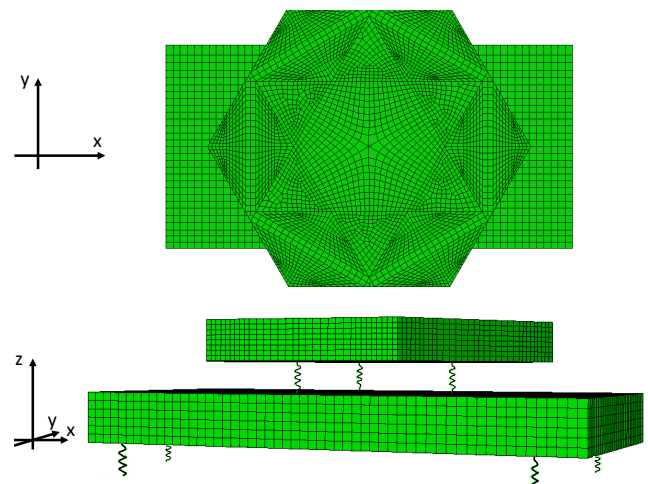
Fig. 1. Top view (top) and front view (bottom) of the FEM of the hexagonal payload. The mesh is finer for the hexagonal table to deal with calculation errors. From the front view, the springs between the two tables are visible.

The outputs are the three directions measured at the nodes

---

[1] J.W., B.D., G.Z. and C.C are with Precision Mechatronics Laboratory, BEAMS Department, Université Libre de Bruxelles, 1050 Brussels, Belgium http://pml.ulb.ac.be/

[2] C.C is with the Department of Aerospace and Mechanical Engineering, Université de Liège, 4000 Liège, Belgium

on top of the hexagonal table, aligned with the springs' nodes. These directions measured allow to recover the signal measured by three pairs of horizontal and vertical sensors. The horizontal sensors are measuring motion oriented with a 120 ° angle from each other. Combined with the three vertical sensors, the six degrees of freedom can be extracted, as needed for the control laws studied here. The pairs of vertical and horizontal actuators are collocated with the springs connecting the two tables together, so no additional input nodes are needed.

The resulting model allows studying the response of the system to an external disturbance with a fast calculation time.

Note that the sensor noise and sensor's dynamics are not included in this study. At low frequency, the sensor noise includes in particular the thermal noise [14]. In addition, below 1 Hz, one principal limitation is the coupling between the signal measured by vertical and horizontal sensors and the tilt motion due to gravity coupling [15], [16]. These limitations represent a challenge to isolate the system in the low-frequency range and will be the subject of a future study.

III. DESIGN OF THE CONTROLLER

The control approach used should allow to isolate actively the 6 degrees of freedom of the hexagonal payload. In fact, equipment like gravitational waves detectors have to be isolated in all directions to operate properly [7], [17]. Here, two MIMO controllers are considered; centralized control and singular value decomposition (SVD) approach. Both methods imply to project the system in a new frame where the controller is designed. These two methods are now going to be detailed following the same steps. First, the new frames are defined and second, the controller designed is presented.

A. Centralized approach

Centralized control consists in controlling the six degrees of freedom independently, i.e. the three degrees of translation and the three degrees of rotation. The plant is projected from the local coordinates of the sensors and actuators into the global coordinates of the payload to isolate. The projection matrices are called the Jacobian matrices. The new plant is

$$G_{cen} = J_s^{-1} G_{dec} (J_a^T)^{-1} \qquad (1)$$

where G_{cen} is the new plant in the centralized coordinates, G_{dec} is the original plant in the local coordinates, J_s is the Jacobian matrix allowing to project the sensor local coordinates in the global coordinates and J_a is the Jacobian matrix allowing to project the actuators local coordinates into the global coordinates.

As explained in section II, the crossover frequency is set between the suspension modes and the flexible modes. This allow having good performance at low-frequency without destabilizing the high-frequency modes. Therefore, for the three translational directions, the gain of the controller is 10^6 and therefore, the crossover frequency is 12 Hz. For the three rotational directions, the gain is 10^5 and the crossover frequency is also 12 Hz for the first rotational directions (θ_x and θ_y) and 8 Hz for the last direction (θ_z). To have

a sufficient phase margin, a lead is designed around each crossover frequency

$$H_{x,y,z,\theta_x,\theta_y} = \frac{20}{6}(s + 2\pi 6)/(s + 2\pi 20) \qquad (2)$$

$$H_{\theta_z} = \frac{15}{4}(s + 2\pi 4)/(s + 2\pi 15) \qquad (3)$$

The controller in the centralized coordinates is a diagonal 6x6 matrix which contains the aforementioned gains and leads, H_{cen}.

In order to compare the two control techniques, they will both be applied to the decentralized plant. The controller for the centralized approach is therefore

$$H_{dec} = (J_a^T)^{-1} H_{cen} J_s^{-1} \qquad (4)$$

B. SVD approach

SVD allows to project the system into a new frame where the system is fully decoupled and the directions obtained are orthogonal to each other [18]

$$G_{dec}(\omega) = U(\omega) \, \Sigma(\omega) \, V^H(\omega) \qquad (5)$$

where $\Sigma(\omega)$ is a diagonal matrix whose elements are the singular values for a specific frequency, $U(\omega)$ is the matrix which allow to project the local sensor coordinates into the coordinates of the singular values for a specific frequency and $V^H(\omega)$ is the projection matrix from the local actuator coordinates to the coordinates of the singular values for a specific frequency.

In order to have real U and V^H projection matrices, the SVD can be applied on a real approximation of the plant [18].

From (5), the SVD has to be applied to all frequencies to decouple the plant at each frequency. However, an approximate decoupling can be performed, i.e., the decomposition is calculated for a given frequency and the projection matrices are applied to the whole frequency range [18]. Here, the approximate decoupling is preferred for reducing computation time. As the crossover frequency will be set around 10 Hz, the SVD will be applied at this frequency to ensure a decoupling of the system around this frequency. The system in the new frame becomes

$$G_{svd} = U^{-1}(\omega_0) \, G_{dec} \, (V^H)^{-1}(\omega_0) \qquad (6)$$

where ω_0 is $2\pi 10$ *rad*/s in this case.

As all directions have to be isolated in the same way, each diagonal term is normalized by its steady state gain and multiplied by 100. From the resulting open-loop, a lead is designed for each diagonal entry to ensure sufficient phase margin at the crossover frequency, resulting in the diagonal controller H_{svd}. The resulting open-loop is shown in figure 2.

In conclusion, to apply this SVD approach to control the decentralized plant, the controller is

$$H_{dec} = (V^H)^{-1}(\omega_0) \, H_{svd} \, U^{-1}(\omega_0) \qquad (7)$$
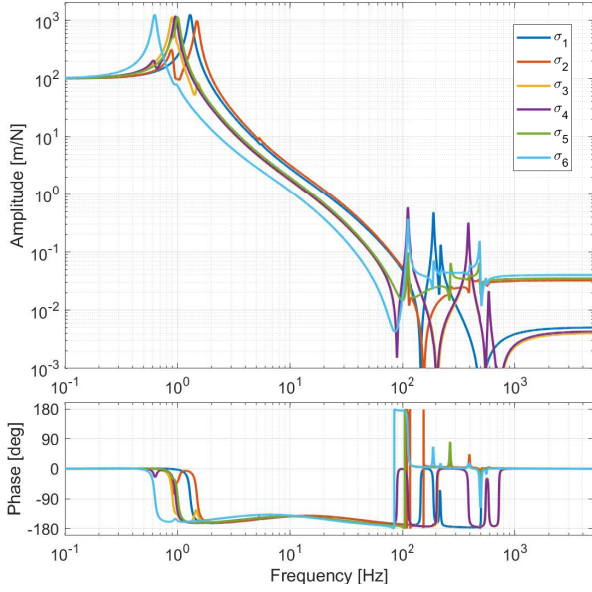
Fig. 2. The six diagonal transfer functions of the open-loop in the frame of the singular values. For each singular value, a lead is designed to provide sufficient phase margin. Almost all directions are decoupled as there is only one resonance at low frequency, except for σ_2 and σ_3.

IV. PERFORMANCE COMPARISON

The active isolation system aims to reduce all environmental disturbances including the transmission of ground motion to the structure. Therefore, the performance has been evaluated on the transmissibility in the horizontal, Fig. 3 and in the vertical direction, Fig. 4. Both control methods allow isolating of a factor 100 the low-frequency range, up to 5 Hz. Moreover, there is no interaction with the flexible modes in both cases. In conclusion, by looking at the diagonal terms, these two MIMO approaches show similar performance.

Note that all the closed-loop poles have a negative real part which guarantees the stability of the closed loop.

To further compare the two methods, the off-diagonal terms have been compared in closed loop. This helps to see how the different signals interact with each other to isolate the system. In Fig. 5, centralized control isolates with one order of magnitude more than with the SVD approach. However, in Fig. 6, the opposite can be observed. Note that, except for two terms, all the off-diagonal terms are at least one order of magnitude lower than the diagonal terms with isolation. Consequently, the off-diagonal terms do not allow to differentiate these two methods neither.

In terms of performance, the two methods are thus equivalent. However, for sake of simplicity, the centralized control was easier to implement which is a non-negligible argument when the controller will be applied experimentally.

V. MODEL VALIDATION

A. Description of the experiment

An experiment has been conducted on a setup that reproduces the features of the FEM detailed in section II. The springs connecting the two tables are isolators from Yuanda
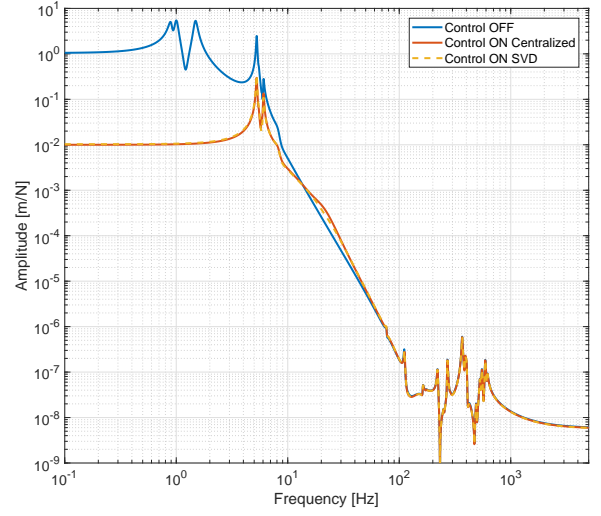
Fig. 3. Transmissibility in the horizontal direction between one sensor on the hexagonal table and a sensor on the ground when no control is applied (solid blue curve), the centralized control is applied (solid red curve) and the control based on the SVD approach is applied (dashed yellow curve).
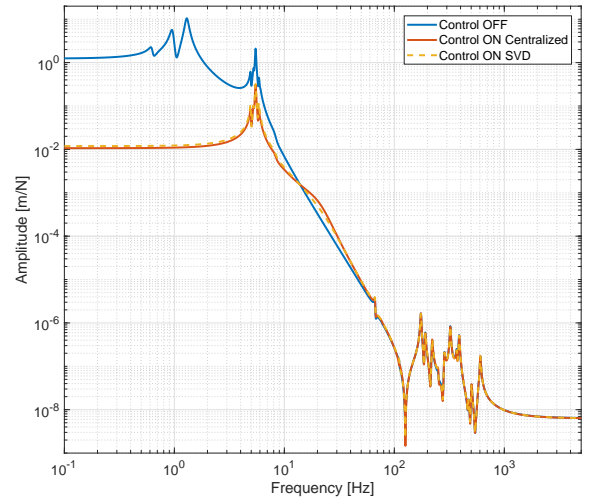
Fig. 4. Transmissibility in the vertical direction between one sensor on the hexagonal table and a sensor on the ground when no control is applied (solid blue curve), the centralized control is applied (solid red curve) and the control based on the SVD approach is applied (dashed yellow curve).

Tech, shown in Fig. 7. Each isolator contains adaptive negative stiffness springs in the vertical. Inside each isolator, there is a pair of horizontal and vertical voice coil actuators. The isolators are designed to support a maximum weight of 100 kg. In order to be in the working range of the isolators, a dummy mass of 70 kg is added at the centre of the payload.

The motion of the table is measured by a Guralp CMG-6T, a geophone that senses the velocity in the three directions. By integrating the signal and multiplying it by the inverse of the sensitivity and the sensor dynamics, the absolute motion of the table can be recovered.

Two sets of experiments have been carried out to identify the system; plant and transmissibility measurements. The plant is the transfer function between an actuator and a sensor. This transfer function is obtained by injecting a
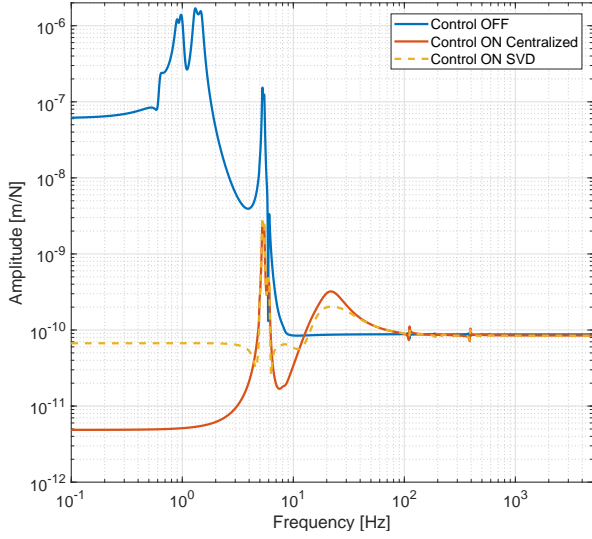
Fig. 5. Transfer function between one vertical sensor and the aligned horizontal actuator when no control is applied (solid blue curve), the centralized control is applied (solid red curve) and the control based on the SVD approach is applied (dashed yellow curve).
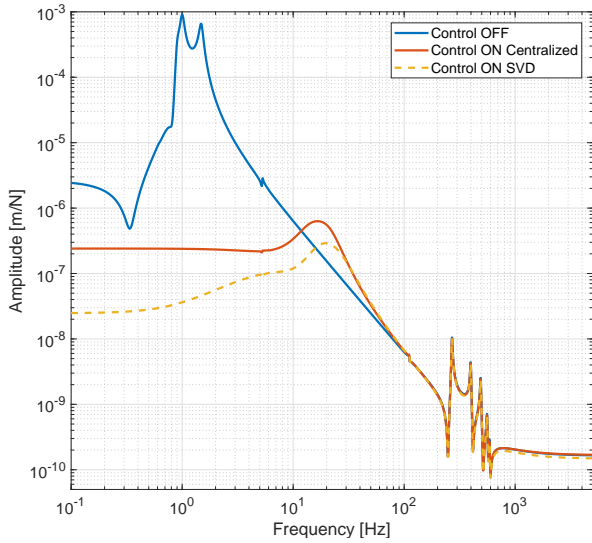
Fig. 6. Transfer function between one horizontal sensor and one non-aligned horizontal actuator when no control is applied (solid blue curve), the centralized control is applied (solid red curve) and the control based on the SVD approach is applied (dashed yellow curve).

white noise signal in an actuator and sensing the motion by a Guralp placed at the location of the sensors defined in section II.

The transmissibility is defined as the transfer function between the ground motion and the payload motion. In this case, a second Guralp CMG-6T was placed on the ground.

B. Experimental results

The plants measured between the vertical sensor and the aligned vertical actuator at the location of each isolator are plotted in Fig. 8. In this graph, the coherence is also plotted to show the quality of the measurement. The suspension modes of the system are around 1 Hz while the flexible modes of

Fig. 7. Picture of the three isolators. A sphere is used to have the smallest contact point between the isolators and the hexagonal table. A guide is put at the centre of mass for safety reasons; there is no contact between the part connected to the hexagonal table and the part fixed to the bottom table except in case of accident.

the system have resonance frequencies above 100 Hz.

In addition, there is a 180° phase shift between some experiment because the signal was sometimes injected in the opposite direction.

The transmissibility in the vertical direction is shown in Fig. 9. the resonances around 1 Hz correspond to the suspension modes of the hexagonal payload while the resonance around 5 Hz is the suspension mode of the rectangular table. In this case, the coherence is only acceptable between 2 Hz and 10 Hz. Outside of this frequency band, the sensors are not sensitive enough. However, this measurement gives us good information regarding the location of the poles as needed for the model validation.

C. Comparison with the Model

The results from the reduced model have been compared to the experimental measurements. In Fig. 8, the model, in dotted line style, has a matching steady-state gain and the resonances and anti-resonances located in the same frequency band. In addition, the flexible modes start at the same high frequencies, above 100 Hz, and some modes are even at the same frequency, see the mode around 100 Hz and around 400 Hz.

In Fig. 9, the transmissibility obtained by the model is plotted in dashed line style. The suspension modes are located in the same frequency band. At high frequency, the model has a roll-off which is not the case of the experimental curve. As explained in section V-A, the coherence of the experimental test is poor at high frequency because the signal is dominated by another source.

Finally, even if not shown here, the off-diagonal terms of the plant measured experimentally and extracted from the model matches; the resonances are in the same frequency band and the behaviour at low and high frequencies are similar.

VI. CONCLUSIONS

In this paper, two MIMO control techniques have been applied on a 6 degrees of freedom model. This model reproduces properly the response of a real system made of
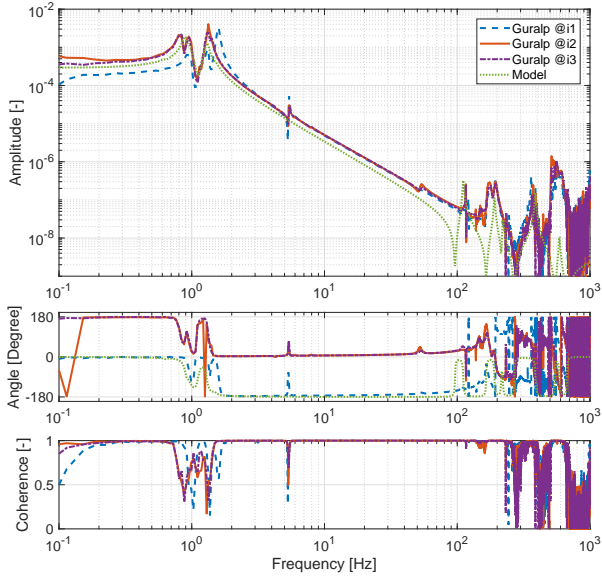
Fig. 8. Transfer functions measured between the vertical motion sensed by the Guralp and the vertical actuator aligned. The "@i1", "@i2" and "@i3" refer to the three different isolators locations. The dotted curve is obtained from the model.
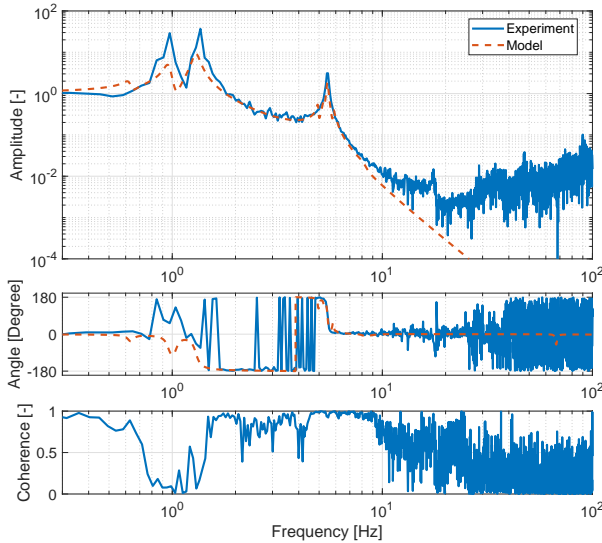
Fig. 9. Transmissibility between a Guralp placed on the hexagonal platform and a Guralp placed on the ground in the vertical direction. The solid line is the experimental measurement and the dashed line corresponds to the model.

a hexagonal table that lays on two series of passive suspensions. Both centralized control and SVD based control lead to the same performance regarding ground motion rejection. However, centralized control is easier to implement.

In order to study the transposability of these control methods on an experiment, the experimental limitations have to be included. First, the plant uncertainty should be added to the model, e.g. by adding some uncertainty on the Jacobian for the centralized control or by adding uncertainty in the high-frequency range. Second, the sensor dynamics can be included, as stated in section II. Once these modifications are

conducted, the control laws will be validated by experimental tests.

REFERENCES

[1] K. K.-L. Miu, A low cost, DC-coupled active vibration isolation system, Ph.D. dissertation, Dept. Mech. Eng., Massachusetts Institute of Technology, Cambridge, MA, 2008.
[2] R. Sugahara, M. Mika and Y. Hiroshi, Performance of an active vibration isolation system, in Proc. International Workshop on Accelerator Alignment, Geneva, 2004, pp. 4-7.
[3] A. Lugungu Ya Zenga, Iterative SISO feedback design for an active vibration isolation system. Traineeship Dissertation, Dept. Mech. Eng., Technische Universiteit Eindhoven, Eindhoven, 2005.
[4] J. van Eijk, D. Laro, J. Eisinger, W. Aarden, T. Michielsen and S. van den Berg, The ultimate performance in floor vibration isolation, Microniek, vol. 51 no 2, 2011, pp. 13-19.
[5] C. Jarvis, Dan Veal, B. Hughes, P. Lovelock, and M. Wagner. 6 degree of freedom micro-vibration test facility for european space agency, presented at ECSSMET, Toulouse, France, 2016.
[6] M.-K. Zhou, X. Xiong, L.-L. Chen, J.-F. Cui, X.-C. Duan and Z.-K. Hu, Note: A three-dimension active vibration isolator for precision atom gravimeters, Review of Scientific Instruments, vol. 86, no. 4, 2015, pp. 046108.
[7] F. Matichard, B. Lantz, K. Mason, R. Mittleman, B. Abbott, S. Abbott, E. Allwine et al., Advanced LIGO two-stage twelve-axis vibration isolation and positioning platform. Part 1: Design and production overview, Precision Engineering, vol. 40, 2015, pp. 273-286.
[8] M. Thier, R. Saathof, A. Sinn, R. Hainisch and G. Schitter, Six degree of freedom vibration isolation platform for in-line nano-metrology, IFACPapersOnLine, vol. 49 no. 21, 2016, pp. 149-156.
[9] J. Pfingstner, M. Hofbauer, D. Schulte and J. Snuverink, SVD-based filter design for the trajectory feedback of CLIC, presented at 2nd International Particle Accelerator Conference, San Sebastian, Spain, 2011.
[10] L. Zuo, Element and system design for active and passive vibration isolation, Ph.D. dissertation, Dept. Mech. Eng., Massachusetts Institute of Technology, Cambridge, MA, 2004.
[11] X.Q. Zhou, D. Y. Yu, X. Shao, S. Wang and S.Q. Zhang, Simplified-super-element-method for analyzing free flexural vibration characteristics of periodically stiffened-thin-plate filled with viscoelastic damping material, Thin-Walled Structures, vol. 94, 2015, pp. 234-252.
[12] A. Deraemaeker, Model reduction in structural dynamics, Precision Mechatronics Lab., Belgium, internal note, 2018.
[13] R. Craig, and M. Bampton, Coupling of substructures for dynamic analyses, AIAA journal, vol. 6 no. 7, 1968, pp. 1313-1319.
[14] P. R. Saulson, Thermal noise in mechanical experiments, Physical Review D, vol. 42 no. 8, 1990, pp. 2437.
[15] B. Lantz, R. Schofield, B. O?Reilly, D. E. Clark, and D. DeBra, Review: Requirements for a Ground Rotation Sensor to Improve Advanced LIGO, Bulletin of the Seismological Society of America, vol. 99, no. 2B, 2009, pp. 980?989.
[16] G. Zhao, B. Ding, J. Watchi, A. Deraemaeker, C. Collette, Experimental study on active seismic isolation using interferometric inertial sensors, Precision Engineering, submitted for publication.
[17] C. M. Mow-Lowry and D. Martynov, A 6D interferometric inertial isolation system, arXiv preprint arXiv, 2018, ref. 1801.01468.
[18] S. Skogestad and I. Postlethwaite, Multivariable feedback control: analysis and design, volume 2. Wiley New York, 2007.